



Wearable multisource quantitative gait analysis of Parkinson's diseases

Junxiao Xie^a, Huan Zhao^a, Junyi Cao^{a,*}, Qiumin Qu^b, Hongmei Cao^b, Wei-Hsin Liao^c, Yaguo Lei^a, Linchuan Guo^a

^a Key Laboratory of Education Ministry for Modern Design and Rotor-Bearing System, School of Mechanical Engineering, Xi'an Jiaotong University, Xi'an, 710049, China

^b Department of Neurology, The First Affiliated Hospital of Medical College of Xi'an Jiaotong University, Xi'an, 710061, China

^c Department of Mechanical and Automation Engineering, The Chinese University of Hong Kong, Shatin, Hong Kong, 999077, China



ARTICLE INFO

Keywords:
Wearable technology
Parkinson's disease
Quantitative analysis
Remote monitoring
Gait abnormalities

ABSTRACT

As the motor symptoms of Parkinson's disease (PD) are complex and influenced by many factors, it is challenging to quantify gait abnormalities adequately using a single type of signal. Therefore, a wearable multisource gait monitoring system is developed to perform a quantitative analysis of gait abnormalities for improving the effectiveness of the clinical diagnosis. To detect multisource gait data for an accurate evaluation of gait abnormalities, force sensitive sensors, piezoelectric sensors, and inertial measurement units are integrated into the devised device. The modulation circuits and wireless framework are designed to simultaneously collect plantar pressure, dynamic deformation, and postural angle of the foot and then wirelessly transmit these collected data. With the designed system, multisource gait data from PD patients and healthy controls are collected. Multisource features for quantifying gait abnormalities are extracted and evaluated by a significance test of difference and correlation analysis. The results show that the features extracted from every single type of data are able to quantify the health status of the subjects ($p < 0.001$, $\rho > 0.50$). More importantly, the validity of multisource gait data is verified. The results demonstrate that the gait feature fusing multisource data achieves a maximum correlation coefficient of 0.831, a maximum Area Under Curve of 0.9206, and a maximum feature-based classification accuracy of 88.3%. The system proposed in this study can be applied to the gait analysis and objective evaluation of PD.

1. Introduction

Parkinson's disease (PD) is one of the typical neurodegenerative diseases associated with irreversible pathological changes. For the purpose of early diagnosis to prevent further development, a multitude of technology-based monitoring measures of Parkinsonian impairments aimed at monitoring previously inaccessible phenomena and early clinical interventions [1,2]. Gait can directly reflect PD patients' gait disorders and is also related to other main symptoms such as tremors, myotonia, and bradykinesia. Therefore, gait monitoring and analysis have become an important research area in the current scenario [3]. In clinical diagnosis, PD symptoms are most often assessed using the movement disorder society-sponsored revision of the unified Parkinson's disease rating scale (MDS-UPDRS) [4], in which scores given by clinicians judge gait abnormalities. This approach, dependent on the experts' judgment, will result in the subjective character of the evaluation. Moreover, slight changes or abnormalities are hard to be captured

by the naked eye. Consequently, quantitative and objective gait measurement methods are gradually developed.

The current objective gait monitoring methods may be classified on the basis of wearability into non-wearable sensor technology (NWST) and wearable sensor technology (WST). NWSTs predominantly use vision and are, therefore, mostly known as vision-based gait monitoring [5–8], with the advantage of being completely contactless. However, NWSTs are environmentally sensitive and only suitable for indoor applications [9]. WSTs generally attach micro or flexible sensors to the human body or clothing to collect motion data through wireless transmission, which tend to be more adapted to daily gait monitoring. More specifically, wearable and wireless transmission modes expand the collected environments from indoors to outdoors or daily life.

To date, the main sensors used in wearable devices for the monitoring of PD or other neurodegenerative disorders include inertial, pressure, and electromyographic (EMG) sensors [10,11]. Inertial sensors are the most widely used of these. Shah et al. arranged three inertial

* Corresponding author.

E-mail address: caojy@mail.xjtu.edu.cn (J. Cao).

sensors in the feet and lumbar region and collected data from 29 PD patients and 27 healthy controls (HC), obtaining individual discriminative measures [12]. There are more similar research efforts monitoring movement parameters in PD patients by arranging inertial sensors in different locations, such as the lower back [13,14], the waist [15–17], the foot [18,19], and multiple joints [20,21]. The next most used is the flexible pressure sensors, which are usually arranged in the insole to capture vertical ground reaction force (vGRF) [22]. The main difference between current devices using pressure sensors is the number of channels and the distribution position of the sensors, e.g., 12 channels per foot [23], 8 channels per foot [24], and multichannel arrays [25]. Moreover, EMG sensors were placed on the human body to record muscle activities [26], such as monitoring muscle tremors to distinguish Parkinson's disease from idiopathic tremors [27] and monitoring leg muscles to distinguish Parkinson's disease [28]. In addition to the above sensing methods, piezoelectric sensors (PER), mainly polyvinylidene fluoride (PVDF) films, are also integrated into insoles [29] or at joints [30] to capture deformation and impact forces. Further, the fusion of multiple sensors provides better performance for health monitoring and diagnosis [31]. Saika et al. demonstrated that combining EMG and electroencephalography sensors could improve the highest diagnosis accuracy than singly used. In Ref. [32], an IoT-based mobile health platform that integrates multiple devices, including pressure sensors, inertial sensors, and smartphones, was developed to monitor multiple symptoms of Parkinson's disease.

Based on the gait data collected by the wearable devices mentioned above, various methods of identifying Parkinson's disease or symptoms have been developed, mainly grouped into the extraction and selection of features with diagnostic capabilities and the construction of algorithmic models for classification and quantification. In terms of the works on feature extraction and analysis, physical features such as pressure amplitude [33], spatiotemporal gait [34], and range of motions [35], and statistical features such as variability and asymmetry of gait parameters [36], were widely calculated and analyzed to reflect abnormalities in Parkinson's disease. In addition, algorithms for Parkinson's disease identification and severity analysis based on machine learning and deep learning methods have achieved good results [37], such as support vector machine algorithms based on trunk acceleration data [38] and vGRF [39], convolutional neural networks and long and short term memory networks based on inertial sensing data and pressure data for the assessment of gait impairment [40–42].

It is noted that the above WSTs provide essential insights into gait signals monitoring and disease analysis. However, there are still some issues. Firstly, human movement information, especially gait, contains abundant and complex information. Whereas a single type of sensor used in current wearable gait monitoring devices can only collect one type of biometric signal, and the gait information collected may not be sufficient for a more accurate diagnosis. Furthermore, to date, there have been few published works on integrating multiple sensors into a single unobtrusive device without strapping for wireless data collection and comprehensive analysis. Secondly, features based on a single type of data can only reflect disease in terms of one physiological signal. Changes in the features of gait data due to Parkinson's disease are currently not fully explored. Moreover, inter-individual non-disease variations make the analysis of features challenging. Clinicians, therefore, need wearable devices to provide more reliable and interpretable digital physiological markers rather than just uninterpretable decision results.

Therefore, a non-invasive and low-cost wearable multisource insole is proposed for quantitative analysis of PD, and the flow of the proposed methodology in this study is shown in Fig. 1. To solve the problem of a single device collecting a single type of data, various sensors, including force sensitive sensors (FSR), piezoelectric sensors (PER), and inertial measurement units (IMU), are integrated into the proposed device with designed circuits. Wireless and remote transmission capabilities enable maneuverability and portability. With the designed system, gait data of

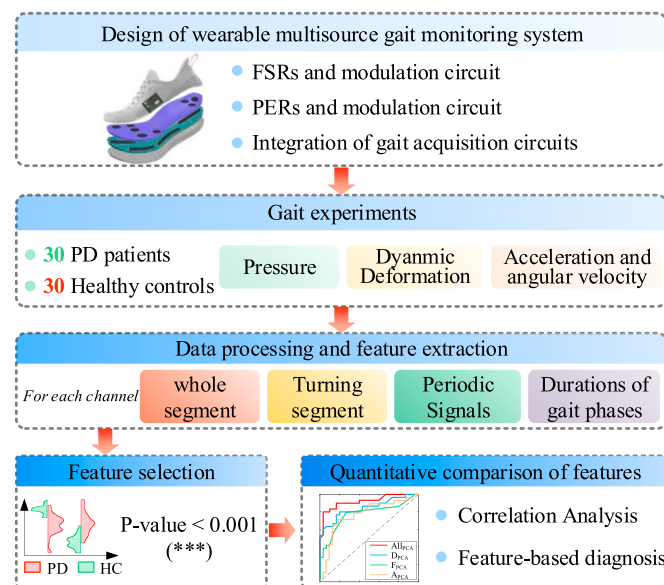


Fig. 1. Flow chart of the proposed method in this study.

30 PD patients and 30 healthy controls are collected. To extract gait-based interpretable and practical digital biomarkers, distinctive features of pressure, dynamic deformation, and postural angle data are obtained based on the knowledge of clinical experts. Finally, evaluations such as Spearman correlation coefficient analysis are performed to investigate the advantage of quantifying PD using wearable multisource gait analysis.

2. Proposed system

2.1. System architecture

The system architecture is sketched in Fig. 2. Due to the fact that the proposed device is designed for daily gait monitoring of the wearers and requires periodic guidance from healthcare professionals, the system should achieve both local monitoring and remote monitoring.

Local monitoring is mainly applied to gait monitoring in daily life or outpatient service in hospitals. In this working scenario, the transmission path of the gait signal is the blue dotted line shown in Fig. 2. Multisource data collected by the wearable device are sent to host devices through a WiFi modem or router. The host devices, such as mobile

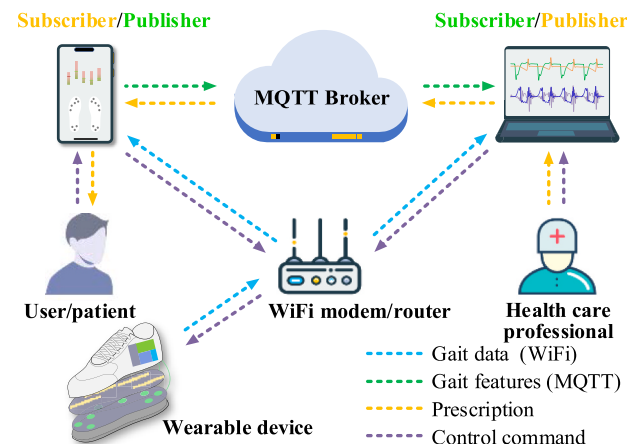


Fig. 2. System architecture. The system consists of a user, a healthcare professional, and a wearable device that enables local and remote monitoring.

phones and laptops, are installed with designed application software. The interface displays gait data waveforms and the selected features' distribution. According to the displayed results, healthcare professionals diagnose PD more accurately in outpatient service, and wearers observe their gait health status in daily life. Moreover, the wearable device can be controlled by host devices, as shown by the purple dotted line.

As PD is one of the chronic, progressive illnesses, regular reinspection is helpful for stabilizing the patients' condition. Therefore, the green dotted lines in Fig. 2 present the function of remote monitoring based on the Message Queuing Telemetry Transport (MQTT) protocol. During remote monitoring, the user's device periodically sends gait features to the MQTT broker as a publisher. The expert-side device acts as a subscriber, obtaining data from the MQTT broker and presenting it. The healthcare professional returns to the user with customized advice based on the health condition, in which case the subscriber and publisher are reversed.

2.2. Wearable multisource device

The wearable device is designed to acquire multi-type and multi-channel signals simultaneously. The composition of the wearable device is shown in Fig. 3. Sensors in the shoe include 8-channel FSRs, 4-channel PERs, and an IMU. FSRs and PERs are flexible films forming the piezoresistive and piezoelectric layers, respectively. The designed signal modulation circuits and a wireless transmission module are integrated into the circuit board attached to the upper of the shoe.

FSRs and modulation circuit: FSR measures vGRF at the corresponding position, and the array of multiple FSRs reflects the distribution and variation of plantar pressure during movement. The changes in plantar pressure are mainly in the posterior heel and anterior foot, where multiple sensors need to be arranged to ensure the collection of sufficient information and reduce the influence of individual variability [33]. The arch and toes also need to be placed with sensors in order to fully reflect the process of plantar pressure changes. Therefore, an 8-channel piezoresistive sensing array is adopted. Each piece of FSR has a diameter of 20 mm with a thickness of 0.45 mm, and the model number is RX-D2027, supplied by RoXi. Fig. 4 shows the distribution of each FSR unit. The plantar pressure at the heel (FSR 1, 2, and 3), arch (FSR 4), sole (FSR 5, 6, 7), and toe (FSR 8) are collected. Since the resistive value of FSR R_F is approximately inversely proportional to the applied pressure, an inverting amplifier circuit is used to regulate signals, as shown in Fig. 5A. The output voltage U_0 of this circuit is equal to $3.3 \cdot R_0/R_F$, so the voltage output obtained by the FSR modulation circuit is linear with respect to the applied pressure. The output voltage of each unit in relation to the applied pressure is calibrated individually by means of a load-unload-load process to guarantee that the output voltage is

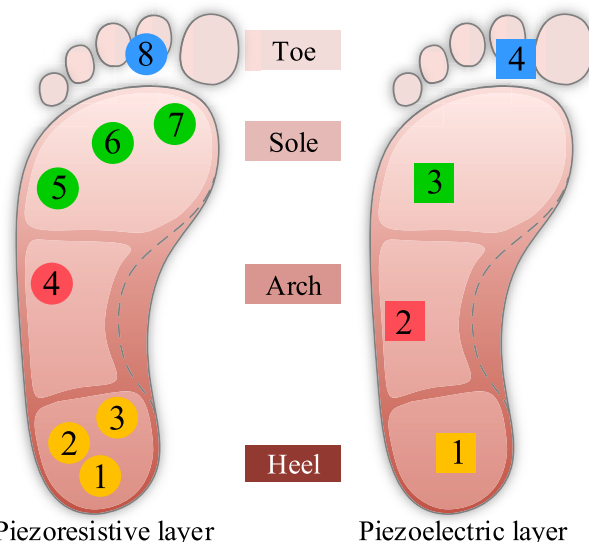


Fig. 4. Distribution of FSRs and PERs. The left side shows the placement of the 8 FSR units, and the right side shows the placement of the 4 PER units in the insole.

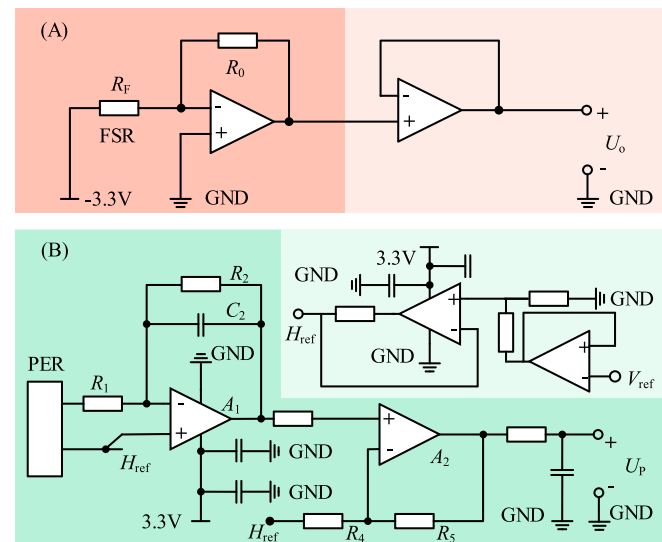


Fig. 5. Modulation circuit for each PER unit and FSR unit. (A) Inverting amplifier circuit for the FSR unit, and (B) amplifying and transforming circuit for the PER unit.

approximately linear with respect to the pressure and the performance is reproducible.

PERs and modulation circuit: PVDF is a type of flexible piezoelectric polymer material that can monitor the change of plantar bend and impact force, and a single PVDF sensor satisfies the acquisition of signals from one area of the foot [29]. In order to monitor the dynamic transition process from heel to toes during walking, four channels of PVDF are arranged in the four main areas, as shown in Fig. 4, including the heel, lateral arch, lateral palm, and toes. In this study, the PERs are made of PVDF supplied by Fils and are $60 * 16 \text{ mm}^2$ strips with a thickness of 0.08 mm.

As the PER sensor outputs a weak charge signal under dynamic load conditions, an amplifying and transform circuit is designed, as shown in Fig. 5B, with reference to the CN-0350 (Analog Devices, USA). The PER unit in Fig. 5B will generate a weak current when subjected to a dynamic

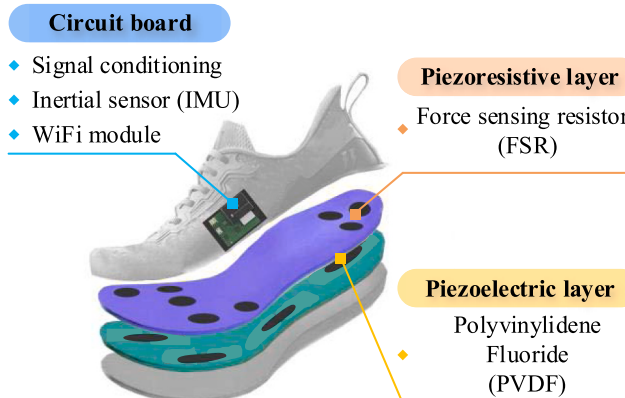


Fig. 3. Composition of the wearable device. The device consists mainly of a piezoelectric layer, a piezoresistive layer, and a circuit board, including an IMU.

deformation, which is converted into a voltage signal U_1 by a current-to-voltage converter consisting of operational amplifier A_1 and capacitor C_2 . Subsequently, the voltage U_1 is amplified by a non-inverting amplifier consisting of operational amplifier A_2 , resistors R_4 , and R_5 with an output voltage U_p . To match U_p to the input range of the AD chip (0–2.5 V), a bias voltage of 1.25 V H_{ref} is added to one end of PER and one end of R_4 and is obtained by buffering and attenuating the 2.5 V reference voltage V_{ref} . The gain of the output voltage U_p in relation to the induced charge Δq is given by

$$U_p = H_{ref} + \left(1 + \frac{R_s}{R_4}\right) \frac{\Delta q}{C_2} \quad (1)$$

where the Δq is directly influenced by both plantar bend and impact force, adjust the value of the resistors and capacitor to control the U_p range from 0 to 2.5 V.

Integrated gait acquisition circuit: The integrated gait acquisition circuit consists of signal modulation circuits, analog-to-digital converters (ADC), a microcontroller, and a wireless transmission module. In terms of signal modulation circuits, in addition to the piezoelectric and piezoresistive signal conditioning circuits, MPU6050 (Invensense, USA), including a 3-axis accelerometer and a 3-axis gyroscope, is chosen as the IMU. IMU monitors the acceleration and angular velocity of the foot, and the entire foot is considered one object when analyzing the IMU signals. Therefore, it is sufficient to arrange one IMU in each of the left and right foot devices. The ADC converts the output of the modulation circuit, including U_0 and U_p , into digital signals and sends them to the microcontroller. In this study, the ADS8321, a multichannel 16-bit, ultralow power analog-to-digital converter provided by Texas Instruments, is applied. Moreover, the ESP32 module is selected as the control core of the system due to the function of the WiFi module and dual-core microcontroller. The gait signals are stored in the controller's cache unit via modulation circuits and ADC and then sent to the host device by the wireless transmission unit. In accordance with the circuits mentioned above, a four-layer PCB is designed with dimensions of 56 mm × 40 mm, as shown in Fig. 6.

2.3. Gait monitoring system and experiments

The wearable gait monitoring system shown in Fig. 6 can collect gait signals at a sampling frequency of 0–1000 Hz. Moreover, it is experimentally verified that the system can work continuously and stably for 24 h to meet daily-wear requirements.

During remote monitoring, data are sent to the online IoT platform



Fig. 6. Wearable gait monitoring system. The system consists of the wearable device and the host computer, where the software receives and processes the wireless data.

inside the Alibaba cloud services via MQTT protocol. Quality of service is set to 2, in which case the protocol guarantees that the message will be received by the broker once and once only, ensuring the necessary reliability to the transmission process [43]. Each wearer's device has a unique ID to allow healthcare professionals to identify patient information and medical records.

In Fig. 6, the monitoring software in the host computer receives data and displays it in real-time. Besides, a gait quantification analysis algorithm for PD is integrated into the software, automatically analyzing the subject's data and thereby extracting the features listed in Chapter 3 to quantify gait abnormalities.

Gait experiments are conducted to collect gait data from patients and healthy elders as a basis for system analysis. The PD patients were admitted to The First Affiliated Hospital of Xi'an Jiaotong University and could walk unaided. The study was approved by the Xi'an Jiaotong University Health Science Center (no.2020-1330) in compliance with the Declaration of Helsinki. All subjects signed the informed consent forms.

30 healthy adults (HC group) and 30 PD patients (PD group) volunteered for this experiment. Subjects with the following conditions are excluded: (i) cannot walk independently and continuously, (ii) suffering from other gait disorders. The experiment requires the subjects to wear gait acquisition devices and walk forth and back in a 30-m-long corridor. Each subject can complete three groups of gait tests at a self-selected speed.

As presented in Table 1, the basic physical characteristics of healthy subjects in the control group are selected to match the PD group. Mann-Whitney *U* test is used to determine whether there is a significant difference ($p < 0.05$). The height, weight, and calf length are roughly consistent between HC and PD groups, whereas there are differences in age and leg length. Subsequent analysis will consider and avoid the effects of basic characteristic differences. In addition, clinical characteristics of PD patients regarding MDS-UPDRS scale scores, scores of the III part in the MDS-UPDRS, and Hoehn & Yahr stages are also demonstrated in Table 1.

3. Feature Extraction and Quantitative Analysis

3.1. Data description and preprocessing

The gait signal during walking is distinctly periodic, with the waveforms of each cycle reflecting the characteristics of the walk. Further analysis of each type of signal is required. Figures and statistical analysis were generated using MATLAB and Statistics Toolbox (release 2021a; The MathWorks Inc., Natick, MA, USA).

FSRs and time phase signals: The plantar pressure waveforms of the left and right feet from the 10th to the 12th second, shown in Fig. 7, are collected simultaneously by gait acquisition devices. It can be seen from Fig. 7 that there are rapid increases in channels 1, 2, and 3 during the first half of the gait cycle, indicating that the heel position is in contact with the ground and under stress. As the body's center of gravity shifts forward during walking, the position of the main force is gradually

Table 1
Information on the 30 PD patients and 30 HC people, including demographic and clinical characteristics.

Subjects (Mean ± SD)	PD (n = 30)	HC (n = 30)	p-value
Gender	18 F, 12 M	16 F, 14 M	0.61
Age (years)	63 ± 9	55 ± 6	0.00098
Weight (kg)	65.08 ± 10.65	66.54 ± 11.47	0.66
Height (cm)	165.1 ± 7.3	161.7 ± 8.7	0.11
Leg length (cm)	89.0 ± 4.1	85.5 ± 4.5	0.0035
Lower leg length (cm)	40.4 ± 2.6	39.5 ± 3.1	0.26
MDS-UPDRS scores	50.3 ± 23.4	—	—
MDS-UPDRS III scores	31.5 ± 15	—	—
Hoehn & Yahr	2.1 ± 0.6	—	—

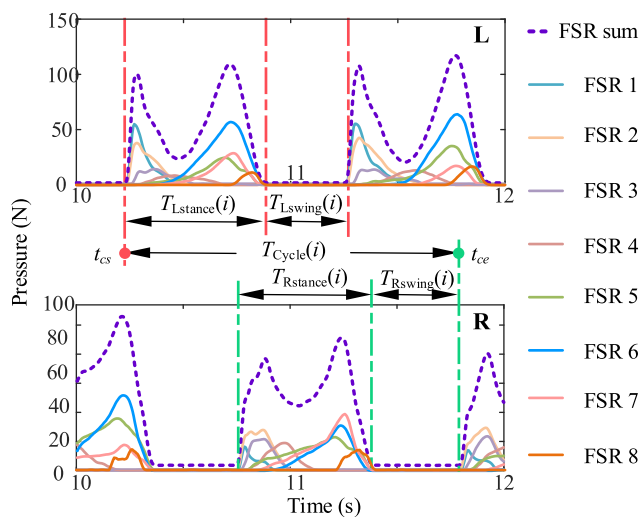


Fig. 7. Plantar pressure signals of feet during a walking period from 10th to 12th seconds. The gait phases and cycles can be divided based on the pressure signal.

shifted from the heel to the arch. The pressures of channels 1, 2, and 3 reach their peaks and then decrease, with the pressure of channel 4 increasing. Then, the position of the main force is shifted from the arch to the sole and toe. At the same time, the pressure of channels 5, 6, 7, and 8 reach their peaks successively. Finally, the foot is raised, and the pressure value in all channels drops to zero. On each foot, the channel FSR sum is the sum of the other eight channel pressures.

The above process represents the gait cycle on one foot and alternates between the right and left feet, as shown in Fig. 7. Depending on whether the foot is touching the ground or not, the gait cycle on one foot can be divided into stance phase and swing phase [33,44], which can be accurately split by the sum of pressures, purple dotted lines in Fig. 7. A complete gait cycle is considered to be from the time the heel of the left foot touches the ground (t_{cs} in Fig. 7) to the time the toes of the right foot leave the ground (t_{ce} in Fig. 7). Thus, the duration of the i -th gait cycle $T_{Cycle}(i)$, the duration of the stance phase ($T_{Lstance}(i)$ for left feet and $T_{Rstance}(i)$ for right feet) and the duration of the swing phase ($T_{Lswing}(i)$ for left feet and $T_{Rswing}(i)$ for right feet) can be calculated and the time series of durations of time phases are shown in Fig. 8. In addition, the time that both feet are on the ground is the double support phase, which equals to $T_{Rstance}(i)-T_{Lswing}(i)$ in the i -th gait cycle.

IMU and postural angle signals: Fig. 9 shows the tri-axial acceleration collected by the acceleration sensor of MPU6050 separately. A_x , a_y , and a_z are the accelerations in the x , y , and z directions. The time segment is the same as in Fig. 7. Nevertheless, MPU6050 is soldered to the board.

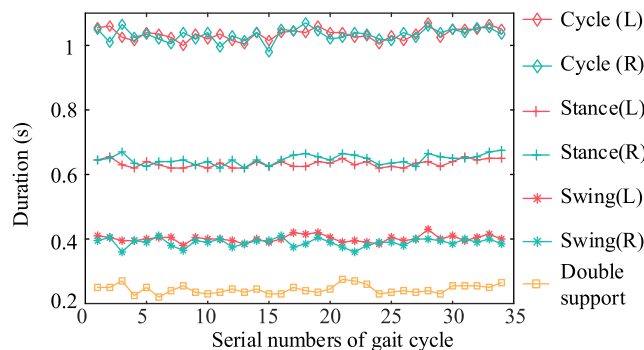


Fig. 8. Gait phase durations of the left foot and right foot at each cycle extracted from a walking signal containing 34 gait cycles.

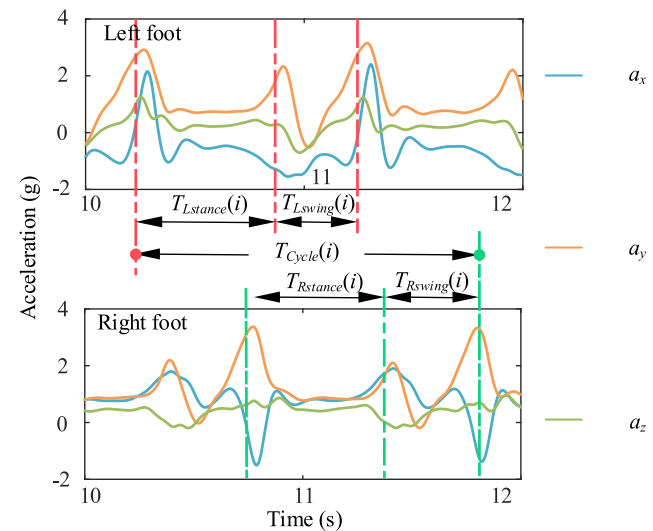


Fig. 9. Acceleration signals of both feet in the IMU coordinate system during walking from the 10th to the 12th seconds.

Although this approach avoids the need to tie the IMU around the lower leg and improves wearing comfort, the data obtained are based on the IMU coordinate system xyz , which is shifted and skewed with movement and needs to be converted to the stationary terrestrial coordinate system, as shown in Fig. 6. In addition to the accelerometer and gyroscope, the MPU6050 incorporates a digital motion processor, which allows direct output of postural angle data of IMU coordinates based on acceleration data and angular velocity data, including roll angle R , yaw angle Y , and pitch angle P .

The rotation of the coordinate system and the conversion process of the data are shown in Fig. 10. The terrestrial coordinate system is rotated around the z , y , and x axes to convert to the IMU coordinate system. The relationship between the angular change measured by IMU can be obtained in (2):

$$\begin{bmatrix} \Delta R \\ \Delta P \\ \Delta Y \end{bmatrix} = M_x M_y \begin{bmatrix} 0 \\ 0 \\ \Delta Y_0 \end{bmatrix} + M_x \begin{bmatrix} 0 \\ \Delta P_0 \\ 0 \end{bmatrix} + \begin{bmatrix} \Delta R_0 \\ 0 \\ 0 \end{bmatrix} = M \begin{bmatrix} \Delta R_0 \\ \Delta P_0 \\ \Delta Y_0 \end{bmatrix} \quad (2)$$

where ΔR , ΔP , ΔY represent changes of postural angle in the IMU coordinate system, ΔR_0 , ΔP_0 , ΔY_0 are the equivalent angular changes, which approximates the angular change in the terrestrial coordinate system and is considered as the postural angular changes. M_x , M_y , and M_z are the three-dimensional Euler angular rotation matrices around the x , y , and z axes, respectively [45].

M is the rotation matrix for which formula (3) is obtained from (2):

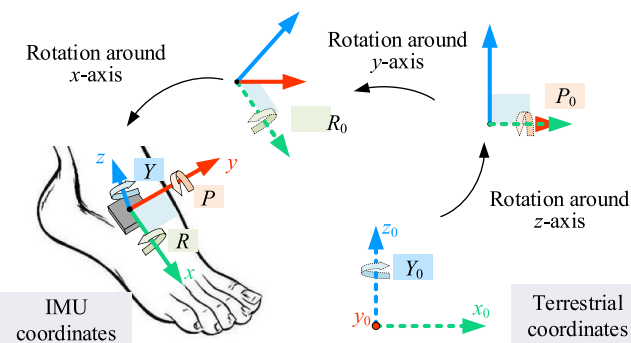


Fig. 10. The rotation of the coordinate system and the conversion process of the angular changes.

$$M = \begin{bmatrix} 1 & 0 & -\sin P_0 \\ 0 & \cos R_0 & \cos P_0 \sin R_0 \\ 0 & -\sin R_0 & \cos P_0 \cos R_0 \end{bmatrix} \quad (3)$$

where R_0 and P_0 are the roll and pitch angles in terrestrial coordinates and are constantly updated with ΔR_0 and ΔP_0 . The initial values of R_0 and P_0 can be calculated from the acceleration of gravity at rest and the rotation matrix:

$$\begin{bmatrix} a_x \\ a_y \\ a_z \end{bmatrix} = g \begin{bmatrix} -\sin(P_0(0)) \\ \cos(P_0(0))\sin(R_0(0)) \\ \cos(P_0(0))\cos(R_0(0)) \end{bmatrix} \quad (4)$$

where a_x , a_y , and a_z are acceleration data collected at rest, equivalent to the acceleration of gravity g in the terrestrial coordinate system. Equation (5) is solved for the initial values $R_0(0)$ and $P_0(0)$ after normalization.

$$\begin{cases} R_0(0) = \arctan\left(\frac{a_y}{a_z}\right) \\ P_0(0) = -\arctan\left(\frac{a_x}{\sqrt{a_y^2 + a_z^2}}\right) \end{cases} \quad (5)$$

Eq. (5) calculates the initial postural angle, which is brought into (2) and (3) to find the angle changes in the ground coordinate system at the next moment. The calculated angular changes are then used to update the matrix M . The calculation process continues to loop until the end of the acquisition. Finally, the postural angle data in the ground coordinate system can be obtained, as shown in Fig. 11. Foot touches the ground and enters the stance phase, and the pitch angle decreases to approximately 0. When the gait changes from the stance phase to the swing phase, the heel is lifted, and the pitch angle decreases rapidly, finally recovering during the swing phase until the next gait cycle. At the same time, there are continuous changes in roll angle and yaw angle throughout the walking process.

PERs and dynamic deformation signals: Fig. 12 displays the voltage data of plantar stress and deformation of the four-channel PERs in each foot after amplification and offset. It reflects the coupled dynamic changes in plantar stress and deformation during walking, referred to as dynamic deformation in the following. The red and green dashed lines represent the division between the stance and swing phases of the left and right foot, in line with Figs. 7 and 9. It can be observed that turns in

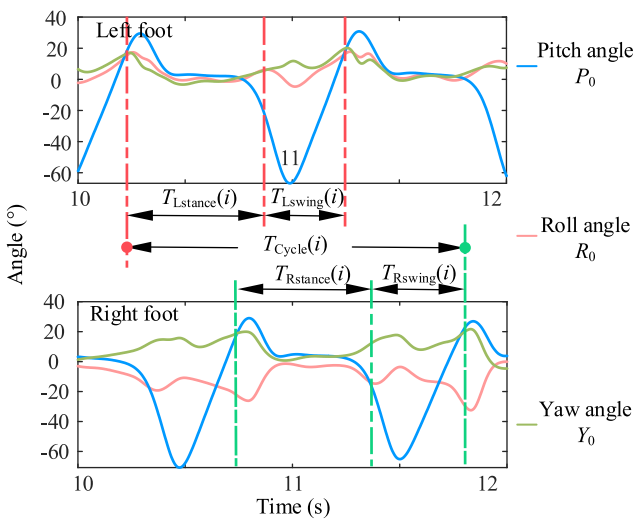


Fig. 11. Postural angles of the feet in the 10th to 12th seconds after transformation. R_0 , P_0 , and Y_0 are approximated angles around the x_0 , y_0 , and z_0 axes in the ground coordinate system.

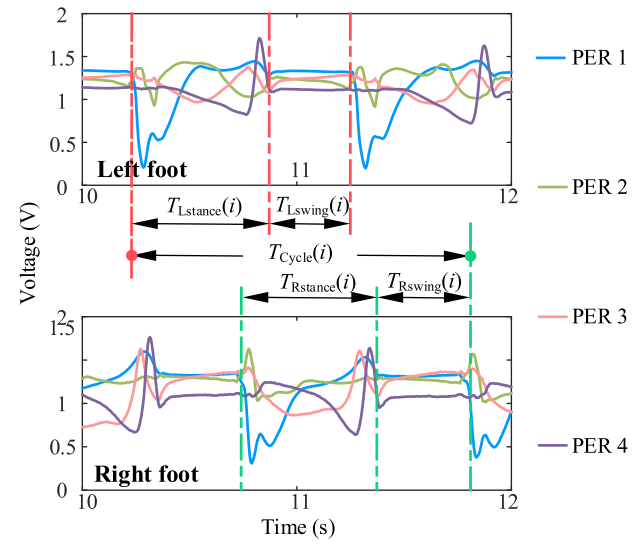


Fig. 12. Dynamic deformation signals of the feet during walking from the 10th to the 12th seconds.

signals accompany changes in gait phases. The signal at the heel drops sharply at the moment of heel strike and then gradually returns to flat. As for the signal at the arch, the signal appears to have a relatively small peak, followed by a depression. The channels 3 and 4 signals peak successively as the palm and toes leave the ground.

3.2. Feature extraction

The relationship between changes in the three types of signals and the walking process is described above and reflects the general pattern of change. To quantify the gait abnormalities of PD patients, the difference between the gait signals of PD and HC needs to be extracted. In this study, the whole, segmental, periodic, and temporal features are extracted from the time, frequency, and time-frequency domains for pressures, postural angles, and dynamic deformation signals, respectively. The detailed feature extraction process is shown in Appendix A.

Means, coefficients of variation (CV), and asymmetry index (AI) are calculated for each periodic sequence consisting of the indicators. CV of a particular feature can be represented as

$$CV_x = \frac{\sqrt{\sum_{i=1}^n |x_i - \frac{1}{n} \sum_{i=1}^n x_i|}}{\frac{1}{n} \sum_{i=1}^n x_i} \quad (6)$$

where CV_x denotes the CV of feature x , reflecting the instability of x over all gait cycles. i refers to the i -th gait cycle and is less than the number of cycles n . x_i can be the duration of the i -th gait phases or the feature values of the collected data during the i -th gait cycle.

AI of feature x is given by

$$AI_x = \frac{\sum_{i=1}^n |x_{l(i)} - x_{r(i)}|}{\frac{1}{2} \left(\sum_{i=1}^n x_{l(i)} + \sum_{i=1}^n x_{r(i)} \right)} \quad (7)$$

where $x_{l(i)}$ and $x_{r(i)}$ are the features of the i -th gait cycle of the left and right foot, respectively.

3.3. Feature analysis

In order to select the features that reflect gait abnormalities, the Mann-Whitney U test is used to determine whether there are significant

differences between the features of the two groups [46]. When indicator p is less than 0.05, it can be assumed that PD patients differ from healthy controls in the corresponding features. For each type of data, features are extracted and analyzed and subsequently ranked according to the value of p . The smaller the p -value, the more significant the difference between PD patients and healthy controls regarding corresponding features.

Among the features extracted from plantar pressure data, the five most distinguishing features are the coefficient of variation of gait cycle duration (DS: CV of T_{cycle}), asymmetry index of swing phase duration (DS: AI of T_{swing}), the mean value of periodic square root amplitude (PS: Mean of X_r) of total plantar pressure, asymmetry index of square root amplitude (PS: AI of X_r) of total plantar pressure, and mean of periodic peak values (Mean of X_p) of hindfoot pressure. Fig. 13 demonstrates the distribution of five pressure features. The green area represents the distribution of normalized eigenvalues of the HC group, whereas the red area belongs to the PD group. In addition, the bar chart region reflects the p -value of the corresponding features. Both CV and AI of DS features are higher overall in the PD group than in the HC group, implying that PD patients walk with weak stability and imbalance in each step. Among them, the CV of T_{cycle} is the most significant, and p equals 1.4×10^{-7} , much less than 0.05. In contrast, the peak values of the pressure are overall smaller in PD.

Five of the features with the most significant differences extracted from dynamic deformation signals are illustrated in Fig. 14. The five most distinguishing features are the coefficient of variation of square root amplitude periodic sequence in channel PER 2 (PS (PER 2): CV of X_r), wavelet scale entropy of the whole signal in channel PER3 (WS (PER 3): wavelet scale entropy), coefficient of variation of waveform indicator periodic sequence in channel PER1 (PS (PER 1): CV of S_f), coefficient of variation of square root amplitude periodic sequence in channel PER1 (PS (PER1): CV of X_r), and mean of the root mean square value periodic sequence in channel PER1 (PS (PER1): Mean of X_{rms}). The difference between the PD and HC groups is mainly found in the periodic signals at the heel (PER 1) and arch (PER 2). The feature CV of X_r , extracted from periodic signals of PER 2, has a minimum p -value of 1.6×10^{-9} . For features evaluating instability and fluctuations, PD patients are generally higher than healthy controls, but for features evaluating dynamic deformation, PD patients have a smaller value. Compared with FSR-based features, PER-based features have smaller p , which means PER-based features are more effective for PD diagnosis.

Fig. 15 shows the distributions of five distinctive features extracted from the postural angle. The five most distinguishing features are the peak-to-peak value of the segmental signal in the channel Yaw (SS (Yaw): V_{p-p}), square root amplitude of the segmental signal in the

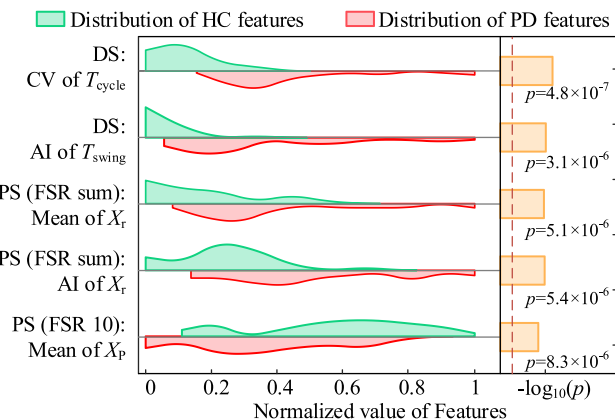


Fig. 13. The features with the most significant differences were extracted from the pressure data. The distributions of the normalized eigenvalues in the PD and HC groups are shown.

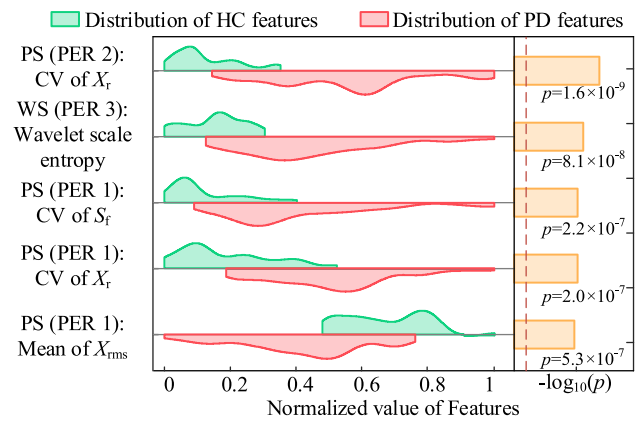


Fig. 14. The features with the most significant differences were extracted from the dynamic deformation data. The distributions of the normalized eigenvalues in the PD and HC groups are shown.

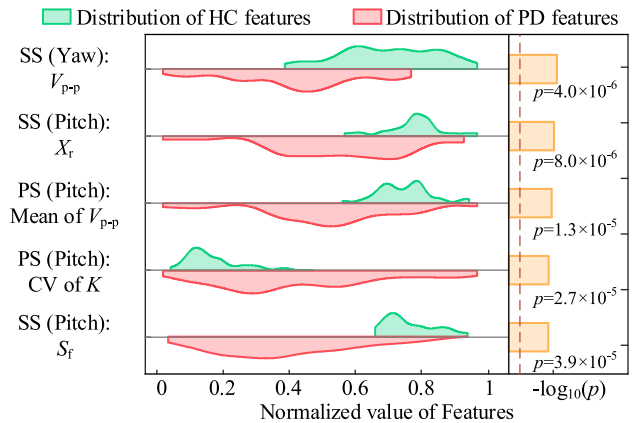


Fig. 15. The distributions of the PD and HC groups on the five most distinctive features extracted from the postural angle.

channel Pitch (SS (Pitch): X_r), mean of peak-to-peak value periodic sequence in channel Pitch (PS (Pitch): Mean of V_{p-p}), coefficient of variation of kurtosis value periodic sequence in channel Pitch (PS (Pitch): CV of K), and waveform indicator of the segmental signal in the channel Pitch (PS (Pitch): S_f). Compared with features of pressure and dynamic deformation, features of postural angle have more mixing between PD and HC. Furthermore, the peak-to-peak value (V_{p-p}) is smaller in the PD group, which may be related to the symptoms of lower limb stiffness during walking. The eigenvalues in terms of the amplitude of the pitch angle, such as X_r of pitch angle and Waveform indicator S_f of pitch angle, in the PD group are smaller than in HC, demonstrating that it is more difficult for PD patients to lift the foot, switching from the stance phase to the swing phase.

The features listed above are significantly different between the HC and PD groups and hence allow us to distinguish the health status of the subjects. For a size of n (n means 60 participants in this study), the n raw feature values f_i and n rows participants' basic information s_i are converted to ranks $R(f_i)$, $R(s_i)$, and Spearman's correlation coefficient ρ is computed as

$$\rho = \frac{\text{cov}(R(f), R(s))}{\sigma_{R(f)} \sigma_{R(s)}} \quad (8)$$

where $\text{cov}(R(f), R(s))$ is the covariance of the rank variables, $\sigma_{R(f)}$ and $\sigma_{R(s)}$ are the standard deviations of the rank variables.

In Table 2, Spearman's correlation coefficients ρ_1 verify that the

Table 2

Spearman's Rank Correlation Analysis of Features. Correlation coefficients between features with demographic and clinical characteristics are calculated.

Data types	Feature	ρ_1	ρ_{Age}	p_{Age}	ρ_{Height}	p_{Height}	ρ_{Weight}	p_{Weight}	ρ_{Leg}	p_{Leg}	ρ_{1Leg}	p_{1Leg}
Pressure	DS: CV of T_{cycle}	0.65	0.03	0.84	-0.11	0.41	0.11	0.39	0.08	0.54	0.22	0.09
	DS: AI of T_{swing}	0.61	-0.01	0.96	0.21	0.11	0.24	0.07	-0.02	0.90	0.16	0.22
	PS(FSR sum): X_r	0.61	0.01	0.92	-0.15	0.27	0.01	0.97	0.07	0.07	-0.18	0.17
	PS(FSR sum): X_p	0.58	-0.05	0.73	-0.12	0.35	-0.20	0.12	0.13	0.32	-0.21	0.11
	AI of X_r	0.54	-0.09	0.51	-0.18	0.18	-0.03	0.83	0.05	0.73	-0.11	0.42
	PS(FSR 10): X_p	0.54	-0.09	0.51	-0.18	0.18	-0.03	0.83	0.05	0.73	-0.11	0.42
Dynamic deformation	PS(PER 2): X_r	0.76	-0.02	0.87	0.23	0.07	0.17	0.19	0.06	0.67	0.19	0.15
	CV of X_r	0.71	-0.05	0.73	0.20	0.13	0.18	0.18	0.08	0.54	0.17	0.21
	WS(PER 3): X_r	0.63	-0.05	0.71	0.13	0.33	0.25	0.06	0.06	0.64	0.15	0.24
	Entropy _{ws}	0.63	-0.05	0.71	0.13	0.33	0.25	0.06	0.06	0.64	0.15	0.24
	CV of S_f	0.61	0.07	0.62	0.17	0.21	0.13	0.34	-0.09	0.51	0.23	0.07
	PS(PER 1): X_r	0.58	0.05	0.71	0.10	0.43	0.15	0.26	-0.04	0.75	-0.07	0.57
Postural angle	Mean of X_{rms}	0.58	-0.05	0.71	0.10	0.43	0.15	0.26	-0.04	0.75	-0.07	0.57
	SS(Yaw): $V_{p,p}$	0.58	-0.11	0.40	-0.22	0.10	-0.14	0.30	-0.10	0.46	-0.14	0.29
	SS(Pitch): X_r	0.56	0.04	0.78	-0.18	0.16	0.13	0.33	0.05	0.72	0.07	0.59
	PS(Pitch): X_r	0.55	0.14	0.29	-0.12	0.37	-0.22	0.10	-0.01	0.94	-0.13	0.34
	Mean of $V_{p,p}$	0.53	0.05	0.71	-0.12	0.36	-0.29	0.02	-0.13	0.34	-0.21	0.12
	CV of K	0.52	-0.06	0.63	-0.22	0.10	-0.13	0.33	0.10	0.44	0.11	0.41

feature values are significantly correlated with the health status of the subjects. The ρ_1 is an index for evaluating the correlation between feature distribution and disease status, equivalent to the p -value. The larger the ρ_1 , the stronger the correlation between feature value and disease. Moreover, Spearman's rank correlation coefficient between the above distinctive features and basic physical characteristics is calculated as shown in Table 2. The p -values obtained from the correlation analysis are all greater than 0.05, and it can be concluded that the extracted features do not correlate with the basic physical characters. Therefore, the variability in age and leg length between the PD groups and HC groups mentioned in Table 1 do not affect the quantification of the features of Parkinson's disease, or the impacts can be ignored.

3.4. Feature analysis based on PhysioBank

To verify the validity of the method and collected data, the proposed feature extraction and selection method is also applied to a public dataset provided by PhysioBank [24]. The dataset contained eight-channel ground reaction forces from 93 PD patients and 73 healthy controls during walking. To match the basic physical characteristics of collected subjects in this work, 30 PD patients and 30 healthy controls are selected only considering gender, age, height, weight, and Hoehn&Yahr. The statistical information results of the subjects are presented in Table 3. The table also shows the statistics of UPDRS scores (the total scores of the patients according to the Unified Parkinson's Disease Rating Scale) and UPDRS-M scores(the scores of the motor symptoms section in the UPDRS) to reflect the severity of the patients.

The pressure features in Table 2 have also been calculated based on

the publicly available database, and their distributions are plotted in Fig. 16, with the blue area representing the HC group and the purple area representing the PD group. In addition, the bar chart region reflects the p -value of the corresponding features. DS: CV of T_{cycle} , DS: AI of T_{swing} , PS(FSR sum): Mean of X_r , PS(FSR sum): AI of X_r , and PS(FSR 10): Mean of X_p are also significantly different between PD group and HC group. What's more, the above features perform consistently in both datasets. The ranges of feature values of the PD group and HC group in this work are respectively consistent with those in the public dataset. According to the distribution curve of each feature within each group in Figs. 13 and 16, it can be seen that the distribution of the feature values calculated by the two datasets is also similar, with a close p -value. Based on the public database, Spearman's rank correlation coefficients between the above features with demographic and clinical characteristics are calculated as shown in Table 4. Therefore, the extracted features are applicable to plantar pressure data, and the ability of quantitative analysis for Parkinson's disease has been demonstrated.

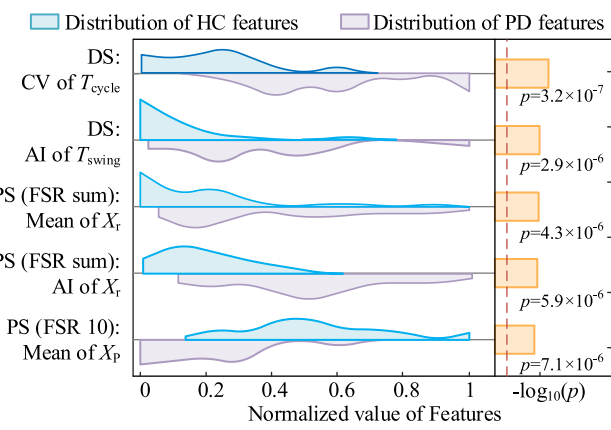


Fig. 16. The distributions of five distinctive features extracted from the publicly available database on plantar pressure.

Table 3
Demographic and clinical characteristics subjects in different groups (PhysioBank).

Subjects (Mean \pm SD)	PD (n = 30)	HC (n = 30)	p
Gender	16 F, 14 M	13F, 17 M	0.45
Age (years)	64 \pm 10	57 \pm 6	0.0016
Weight (kg)	72.6 \pm 13.4	71.8 \pm 12.6	0.83
Height (cm)	166.7 \pm 8.9	166.4 \pm 8.1	0.89
UPDRS scores	30 \pm 12.7	—	—
UPDRS-M scores	19.1 \pm 8.116	—	—
Hoehn & Yahr	2 \pm 0	—	—

Table 4

Spearman's rank correlation analysis of features based on publicly available pressure database.

Data types	Feature	ρ_1	ρ_{Age}	p_{Age}	ρ_{Height}	p_{Height}	ρ_{Weight}	p_{Weight}	ρ_{Leg}	p_{Leg}	ρ_{L_Leg}	p_{L_Leg}
Pressure (PhysioBank)	DS:	0.63	-0.11	0.39	0.13	0.34	0.03	0.82	-	-	-	-
	CV of T_{cycle}											
	DS:	0.61	-0.14	0.27	0.09	0.48	-0.02	0.87	-	-	-	-
	AI of T_{swing}											
	PS(FSR sum): X_r	0.60	-0.16	0.23	0.10	0.43	0.01	0.98	-	-	-	-
	PS(FSR sum): AI of X_r	0.58	0.07	0.62	-0.20	0.12	0.06	0.64	-	-	-	-
	PS(FSR 10): X_p	0.55	0.03	0.84	0.04	0.74	0.04	0.74	-	-	-	-

3.5. Quantitative comparison of features

According to the above analysis, there are overlapped zooms in all features. It is obvious that the feature values of some PD patients are equal to those of the HC group in some cases. This is mainly due to the fact that complex, multitype, and even opposite gait abnormalities may be caused by PD [47], and one patient cannot suffer from all the symptoms. In terms of differences in only a single feature, PER-based features have the most distinctive difference, followed by pressure features, and the last is IMU-based features. Nevertheless, single features are not sufficient to reflect the ability to quantify Parkinson's disease for each type of data comprehensively. Therefore, for each type of data, features satisfying that p -value is less than 0.001 are input to the principal component analysis (PCA) to obtain a composite feature, reflecting the overall effect of the signal.

The performance of the features used for the diagnosis of PD is compared in Table 5. P_{PCA} , D_{PCA} , A_{PCA} , and All_{PCA} are the comprehensive features obtained by PCA of pressure features in Fig. 13, dynamic deformation features in Fig. 14, postural angle features in Fig. 15, and all of the features, respectively. In addition, the features with the smallest p -value among the three types of data are also analyzed, including P_1 (DS: CV of T_{cycle}) in pressure data, D_1 (CV of X_r extracted from periodic signals of PER 2) in dynamic deformation data, and A_1 (SS(Yaw): V_{p-p}) in postural angle data. The Spearman correlation coefficient ρ quantifies the correlation between the above features and the presence or absence of PD. It can be seen that the proposed features provide better disease identification with a larger Spearman correlation coefficient ρ after dimensionality reduction by PCA. For three types of features, D_{PCA} has the maximum ρ , indicating that dynamic deformation signals can best reveal the differences between PD and HC groups by the feature extraction and analysis method in this work. Moreover, the ρ of All_{PCA} is the maximum, reaching 0.831, illustrating that the features obtained by combining the three types of signals are most closely correlated with the health status of subjects.

In binary classification, true positives (TP), false positives (FP), false negatives (FN), and true negatives (TN) represent classification results. Sensitivity (equals to $TP/(TP + FN)$) and specificity (equals to $TN/(TN + FP)$) represent the algorithms' capability to detect TP and TN, and accuracy (equals to $(TN + TP)/(TP + FP + TN + FN)$) summarizes the performance of a classification model as the percentage of correct

predictions [37]. To analyze the ability of each feature to classify healthy controls and PD patients, the threshold for classification of the normalized features is varied from 0 to 1 with a step of 0.005, and the accuracy, sensitivity, and specificity corresponding to each step are obtained. Finally, the receiver operating characteristic (ROC) curves are obtained. As shown in Fig. 17, the ROC curves for each feature are plotted, and the Area Under Curve (AUC) is used as a more intuitive criterion to represent the performance of features to identify Parkinson's disease, and the results are listed in Table 5. The optimal threshold value β for each feature maximizes the sum of sensitivity and specificity, so the optimal threshold for each feature and the corresponding performance evaluation metrics are calculated as presented in Table 5. From the ROC curves, it can be found that features slightly improve the classification accuracy after PCA for every single data type. When features from all three types of signals are used simultaneously, the AUC achieves 0.9206. This method, which uses the features from all three signals simultaneously, has an accuracy of 88.3%, a sensitivity of 80%, and a specificity of 96.7%. The analysis results demonstrate that collected multisource gait data can adequately represent gait abnormalities.

Additionally, compared to previous work, the features we obtained by fusing the multisource signals have a higher performance in PD classification. In the previous work of Shah et al. [12], they obtained a maximum AUC of 0.89 based on the features extracted from data collected by inertial sensors. Also, based on IMUs, 14 IMUs were arranged, and the p -values of the obtained discriminative features were less than 0.001 [20]. In terms of pressure data, Zhao et al. [29] obtained p -values of about 0.001 and accuracies of between 77% and 93% with base classifiers using a public database in PhysioNet. Overall, at the feature level, the features we extracted have more significant differences, especially supported by multiple sources of data. Interpretable algorithms based on this work are yet to be developed to improve the classification performance further.

These findings are understandable because the extracted features can reflect the gait abnormalities of PD from multiple mechanistic perspectives of pressure, dynamic deformation, durations of gait phases, and postural angles. More types of data and features are more likely to be associated with complex gait abnormality symptoms. Therefore, the ability of collected multisource gait data for the diagnosis of Parkinson's disease is validated.

4. Conclusion

For daily monitoring and quantitative analysis of Parkinson's disease, an IoT wearable multisource gait monitoring system is proposed, and features for quantitative analysis of gait abnormalities are extracted.

8-channel FSRs, 4-channel PERs, and IMU sensors are integrated into the proposed device. Through the design of the signal modulation circuit and building of the wireless transmission framework, the real-time acquisition and wireless transmission of multisource signals are achieved in both local and remote monitoring. With the designed system, multisource gait data of 30 Parkinson's patients and 30 healthy controls are collected and analyzed. The relationship between the collected data,

Table 5

Feature-based performance for Parkinson's disease identification, including Spearman's correlation coefficient, AUC, accuracy, sensitivity, and specificity.

Feature	ρ	AUC	Accuracy	Sensitivity	Specificity	β
P_1	0.645	0.7589	73.3%	73.3%	73.3%	0.41
P_{PCA}	0.742	0.7789	76.7%	80.0%	73.3%	0.02
D_1	0.760	0.7987	76.7%	86.2%	66.7%	0.39
D_{PCA}	0.796	0.8444	80.0%	80.0%	80%	0.19
A_1	0.687	0.7456	71.7%	56.7%	86.7%	0.31
A_{PCA}	0.707	0.7645	76.7%	71.4%	81.2%	0.70
All_{PCA}	0.831	0.9206	88.3%	80.0%	96.7%	0.45

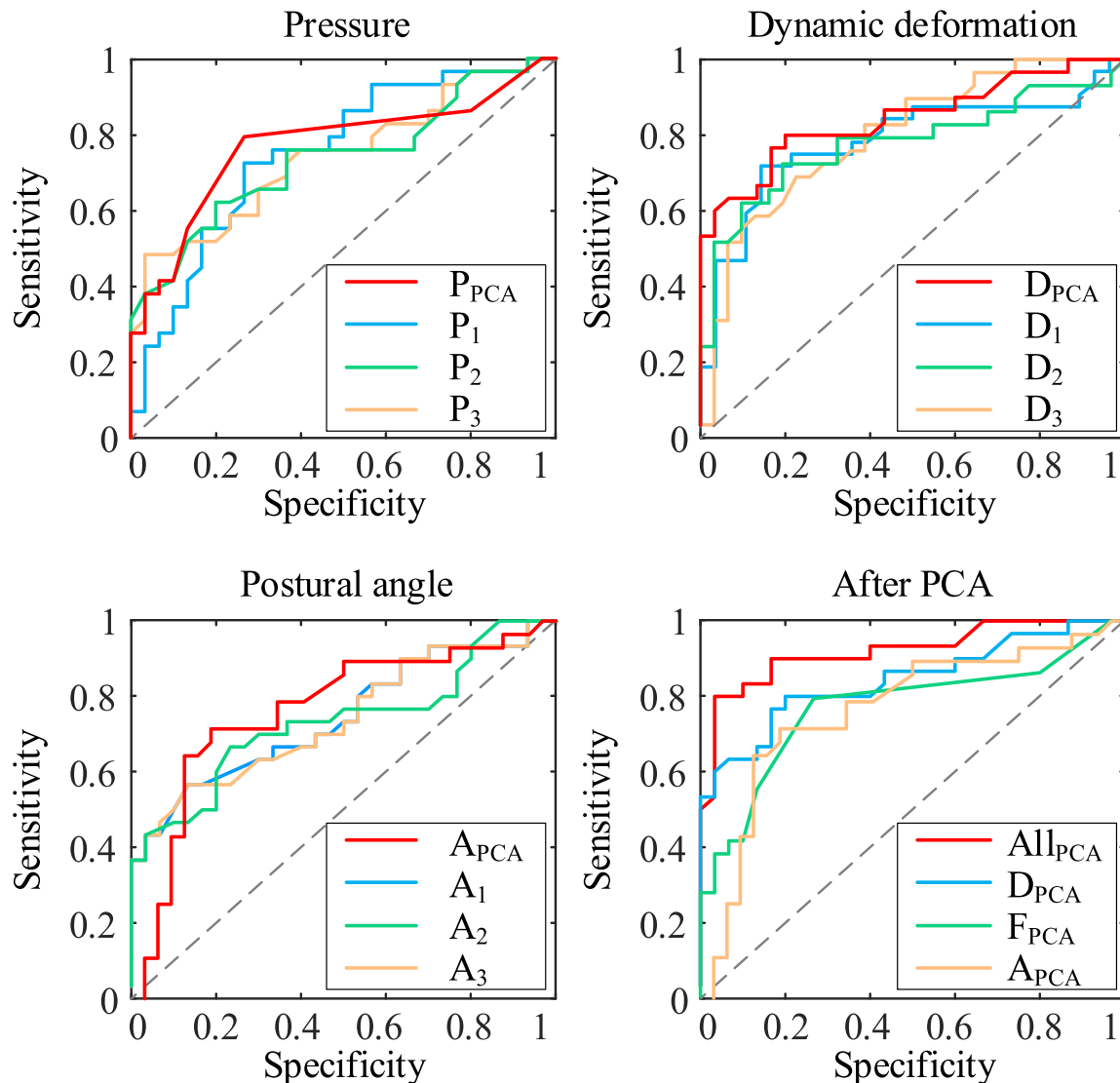


Fig. 17. ROCs based on features of pressure, dynamic deformation, postural angle signals, and fusion of the three signals. Feature All_{PCA} achieves the best result.

including pressure, duration of gait phase, dynamic deformation, and postural angle, with the actual walking process is revealed. Based on the multisource data, distinctive features indicating the corresponding gait abnormalities are extracted by statistical analysis.

The results show that all three types of signals have the diagnostic capability for Parkinson's disease. Herein, quantitative diagnosis based on dynamic deformation features works best, with ρ reaching 0.796 and AUC reaching 0.8444. Followed by pressure features ($\rho = 0.742$ and AUC = 0.7789), and the last are postural angle features ($\rho = 0.587$ and AUC = 0.7645). Moreover, the collected pressure data achieves consistent results with the public datasets, with similar distributions in the same features that quantify PD. More importantly, the fusion of multi-source gait data enables mutual complementation and better recognition than single-source data. When multisource gait data are used simultaneously, Spearman's ranks correlation coefficient reaches 0.831, and the AUC reaches 0.9206.

Appendix A. Process of feature extraction

Fig. A1 illustrates the feature extraction process with an example of a pressure signal, including whole, segmental, periodic, and temporal features.

The proposed wearable multisource gait quantitative analysis method will be helpful for laying an important foundation for the quantitative clinical diagnosis of Parkinson's disease in the future.

Declaration of competing interest

None declared.

Acknowledgments

This work was supported by the National Key Research and Development Program of China [Grant No. 2021YFE0203400] and Innovation and Technology Commission under Mainland-Hong Kong Joint Funding Scheme (MHKJFS), the Hong Kong Special Administrative Region, China [Project No. MHP/043/20].

For whole segment signals and segment signals during turns, the features in the table are calculated directly based on the data of each channel and are named WS (channel number): Feature name and SS (channel number): Feature name, respectively. For periodic signals (PS) and durations of gait phases (DS), the signal of each channel is first divided according to gait cycles and gait phases, which are identified based on the pressure values of the total plantar pressure channel (FSR sum). Then, the features in the table are extracted for each cycle, and ten cycles of features are selected to form a feature sequence, selecting three times with different cycles selected each time. Finally, the coefficient of variation (CV), asymmetry index (AI), and the mean values of the feature sequences are calculated according to eq. (6) and eq. (7), and the results of the three sets of sequences were averaged. The table on the right side of the figure lists the time domain features and frequency domain features used. In addition to this, wavelet entropy features are also calculated.

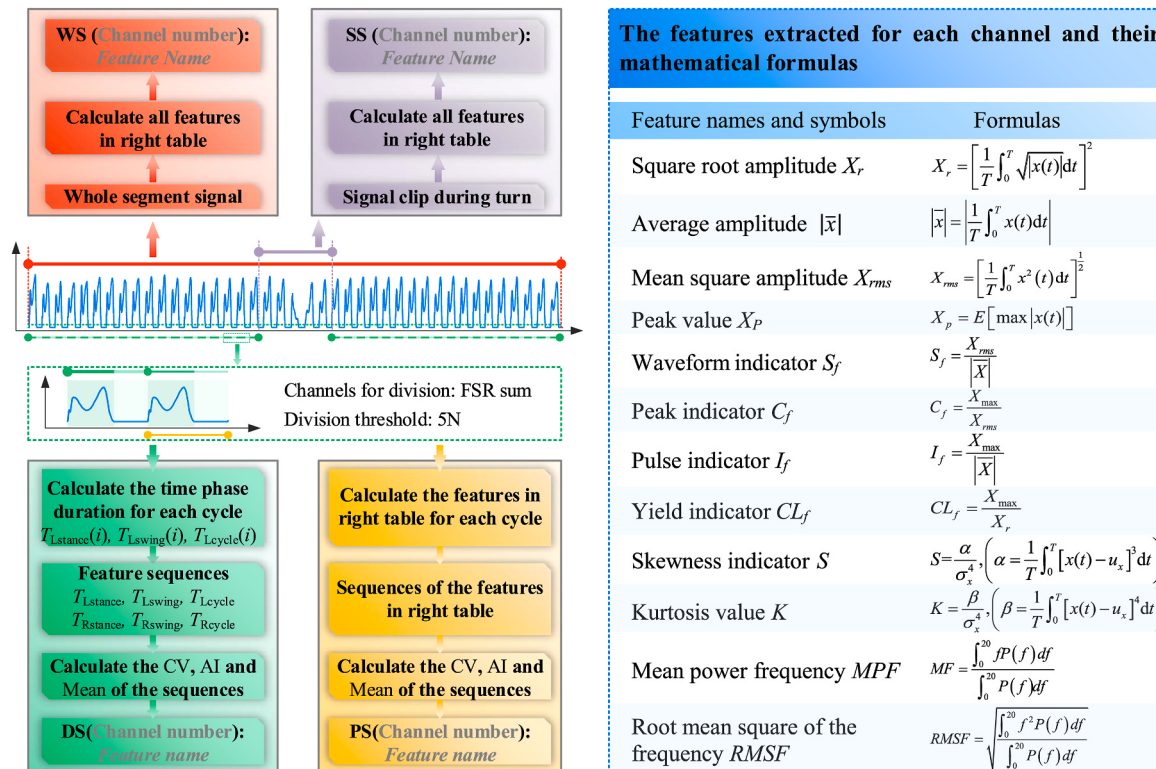


Fig. A1. The process of extracting features from the whole, turn segment, period, and time phase. The right half shows the formulas for some of the time domain features and frequency domain features.

Acronyms

PD	Parkinson's disease
MDS-UPDRS	Movement Disorder Society-sponsored revision of the unified Parkinson's disease rating scale
NWST	non-wearable sensor technology
WST	wearable sensor technology
EMG	electromyographic
HC	healthy controls
vGRF	vertical ground reaction force
PER	Piezoelectric sensors
PVDF	polyvinylidene fluoride
FSR	force sensitive sensor
IMU	inertial measurement unit
MQTT	Message Queuing Telemetry Transport
ADC	analog-to-digital converter
WS	whole segment signal
SS	segmental signal
PS	periodic signal
DS	durations of gait phase
CV	coefficient of variation
AI	asymmetry index
UPDRS	Unified Parkinson's Disease Rating Scale

References

- [1] A.J. Espay, et al., Technology in Parkinson's disease: challenges and opportunities, *Mov. Disord.* 31 (9) (2016) 1272–1282.
- [2] H. Wang, et al., Guest editorial: Special issue on Internet of Things for smart and connected health, *IEEE Internet Things J.* 2 (1) (2015) 1–4.
- [3] N. Kour, S. Gupta, S. Arora, Sensor technology with gait as a diagnostic tool for assessment of Parkinson's disease: a survey, *Multimed. Tool. Appl.* (2022) 1–37.
- [4] C.G. Goetz, et al., Movement disorder society-sponsored revision of the unified Parkinson's disease rating scale (MDS-UPDRS): scale presentation and clinimetric testing results, *Mov. Disord.* 23 (15) (2008) 2129–2170.
- [5] A. Sepas-Moghadam, A. Etemad, Deep gait recognition: a survey, *IEEE Trans. Pattern Anal. Mach. Intell.* 45 (1) (2022) 264–284.
- [6] K.-D. Ng, S. Mehdizadeh, A. Iaboni, A. Mansfield, A. Flint, B. Taati, Measuring gait variables using computer vision to assess mobility and fall risk in older adults with Dementia, *IEEE J Transl Eng Health Med* 8 (2020) 1–9.
- [7] A. Ali, K. Sundaraj, B. Ahmad, N. Ahmed, A. Islam, Gait disorder rehabilitation using vision and non-vision based sensors: a systematic review, *Bosn. J. Basic Med. Sci.* 12 (3) (2012) 193–202.
- [8] A. Kleiner, et al., The coefficient of friction in Parkinson's disease gait, *Funct. Neurol.* 32 (1) (2017) 17–22.
- [9] C. Chen, J. Liang, H. Zhao, H. Hu, J. Tian, Frame difference energy image for gait recognition with incomplete silhouettes, *Pattern Recogn. Lett.* 30 (11) (2009) 977–984.
- [10] H. Zhao, et al., Wearable sensors and features for diagnosis of neurodegenerative diseases: a systematic review, *Digital Health* 9 (2023), 20552076231173570.
- [11] W. Tao, T. Liu, R. Zheng, H. Feng, Gait analysis using wearable sensors, *Sensors* 12 (2) (2012) 2255–2283.
- [12] V.V. Shah, et al., Digital biomarkers of mobility in Parkinson's disease during daily living, *J. Parkinsons Dis.* 10 (2020) 1099–1111.
- [13] H.R. Gonçalves, A. Rodrigues, C.P. Santos, Gait monitoring system for patients with Parkinson's disease, *Expert Syst. Appl.* 185 (2021), 115653.
- [14] A. Rodríguez-Molinero, et al., Analysis of correlation between an accelerometer-based algorithm for detecting Parkinsonian gait and UPDRS subscales, *Front. Neurol.* 8 (2017) 431.
- [15] M. Yoneyama, Y. Kurihara, K. Watanabe, H. Mitoma, Accelerometry-based gait analysis and its application to Parkinson's disease assessment— Part 2 : a new measure for quantifying walking behavior, *IEEE Trans. Neural Syst. Rehabil. Eng.* 21 (6) (2013) 999–1005.
- [16] H. Terashi, T. Taguchi, Y. Ueta, Y. Okubo, H. Mitoma, H. Aizawa, Analysis of non-invasive gait recording under free-living conditions in patients with Parkinson's disease: relationship with global cognitive function and motor abnormalities, *BMC Neurol.* 20 (1) (2020) 1–7.
- [17] A. Sama, et al., Estimating bradykinesia severity in Parkinson's disease by analyzing gait through a waist-worn sensor, *Comput. Biol. Med.* 84 (2017) 114–123.
- [18] J. Stamatakis, J. Crémers, D. Maquet, B. Macq, G. Garraux, Gait feature extraction in Parkinson's disease using low-cost accelerometers, in: 2011 Annual International Conference of the IEEE Engineering in Medicine and Biology Society, 2011, pp. 7900–7903.
- [19] R. Hua, Y. Wang, Distinguishing medication ON and OFF for Parkinson's disease through repetitive foot motion recognition and analysis, *IEEE Sensor. J.* 22 (2022) 12219–12227.
- [20] M. Ricci, G. Di Lazzaro, A. Pisani, N. Mercuri, F. Giannini, G. Saggio, Assessment of motor impairments in early untreated Parkinson's disease patients: the wearable electronics impact, *IEEE J Biomed Health Inform* 24 (1) (2019) 120–130.
- [21] Y. Guo, et al., High-accuracy wearable detection of freezing of gait in Parkinson's disease based on pseudo-multimodal features, *Comput. Biol. Med.* 146 (2022), 105629.
- [22] R. Das, S. Paul, G.K. Mourya, N. Kumar, M. Hussain, Recent trends and practices toward assessment and rehabilitation of neurodegenerative disorders: insights from human gait, *Front. Neurosci.* 16 (2022).
- [23] A. Howell, T. Kobayashi, H. Hayes, K. Foreman, S. Bamberg, Kinetic gait analysis using a low-cost insole, *IEEE Trans. Biomed. Eng.* 60 (12) (2013) 3284–3290.
- [24] A. Goldberger, PhysioToolkit PhysioBank, Physionet : components of a new research resource for complex physiologic signals, *Circulation* 101 (23) (2000) e215–e220.
- [25] G. Shalin, S. Pardoel, E.D. Lemaire, J. Nantel, J. Kofman, Prediction and detection of freezing of gait in Parkinson's disease from plantar pressure data using long short-term memory neural-networks, *J. NeuroEng. Rehabil.* 18 (2021) 167.
- [26] J. Ryu, D.-H. Kim, Real-time gait subphase detection using an EMG signal graph matching (ESGM) algorithm based on EMG signals, *Expert Syst. Appl.* 85 (2017) 357–365.
- [27] V. Ruonala, et al., EMG signal morphology and kinematic parameters in essential tremor and Parkinson's disease patients, *J. Electromyogr. Kinesiol.* 24 (2014) 300–306.
- [28] E. Scholz, H.C. Diener, J. Noth, H. Friedemann, J. Dichgans, M. Bacher, Medium and long latency EMG responses in leg muscles: Parkinson's disease, *J. Neurol. Neurosurg. Psychiatry* 50 (1987) 66–70.
- [29] H. Zhao, R. Wang, D. Qi, J. Cao, W.-H. Liao, Wearable gait monitoring for diagnosis of neurodegenerative diseases, *Measurement* 202 (2022), 111839.
- [30] Y. Cha, H. Kim, D. Kim, Flexible piezoelectric sensor-based gait recognition, *Sensors* 18 (2) (2018) 468.
- [31] C. Virginia Anikwe, et al., Mobile and wearable sensors for data-driven health monitoring system: state-of-the-art and future prospect, *Expert Syst. Appl.* 202 (2022), 117362.
- [32] K.M. Tsioris, et al., PD_Manager: a mHealth platform for Parkinson's disease patient management, *Healthc Technol Lett* 4 (2017) 102–108.
- [33] H. Zhao, J. Cao, R. Wang, Y. Lei, W.-H. Liao, H. Cao, Accurate identification of Parkinson's disease by distinctive features and ensemble decision trees, *Biomed. Signal Process Control* 69 (2021), 102860.
- [34] E. Balaji, D. Brindha, V.K. Elumalai, K. Umesh, Data-driven gait analysis for diagnosis and severity rating of Parkinson's disease, *Med. Eng. Phys.* 91 (2021) 54–64.
- [35] C. Caramia, et al., IMU-Based classification of Parkinson's disease from gait: a sensitivity analysis on sensor location and feature selection, *IEEE J Biomed Health Inform* 22 (2018) 1765–1774.
- [36] M.I.A. Ferreira, F.A. Barbieri, V.C. Moreno, T. Penedo, J.M.R. Tavares, Machine learning models for Parkinson's disease detection and stage classification based on spatial-temporal gait parameters, *Gait Posture* 98 (2022) 49–55.
- [37] L. Sigcha, et al., Deep learning and wearable sensors for the diagnosis and monitoring of Parkinson's disease: a systematic review, *Expert Syst. Appl.* 229 (2023), 120541.
- [38] D. Trabassi, et al., Machine learning approach to support the detection of Parkinson's disease in IMU-based gait analysis, *Sensors* 22 (2022) 3700.
- [39] F. Setiawan, C.-W. Lin, Identification of neurodegenerative diseases based on vertical ground reaction force classification using time–frequency spectrogram and deep learning neural network features, *Brain Sci.* 11 (2021) 902.
- [40] X. Liu, W. Li, Z. Liu, F. Du, Q. Zou, A dual-branch model for diagnosis of Parkinson's disease based on the independent and joint features of the left and right gait, *Appl. Intell.* 51 (2021) 7221–7232.
- [41] C.-H. Lin, F.-C. Wang, T.-Y. Kuo, P.-W. Huang, S.-F. Chen, L.-C. Fu, Early detection of Parkinson's disease by neural network models, *IEEE Access* 10 (2022) 19033–19044.
- [42] C. Fernandes, et al., Discrimination of idiopathic Parkinson's disease and vascular parkinsonism based on gait time series and the levodopa effect, *J. Biomech.* 125 (2021), 110214.
- [43] V. Bianchi, M. Bassoli, G. Lombardo, P. Fornaciari, M. Mordonini, I. De Munari, IoT wearable sensor and deep learning: an integrated approach for personalized human activity recognition in a smart home environment, *IEEE Internet Things J.* 6 (5) (2019) 8553–8562.
- [44] R. Liu, et al., A wearable gait analysis and recognition method for Parkinson's disease based on error state Kalman filter, *IEEE J Biomed Health Inform* 26 (8) (2022) 4165–4175.
- [45] J. Diebel, Representing attitude: euler angles, unit quaternions, and rotation vectors, *Matrix* 58 (15–16) (2006) 1–35.
- [46] N. Nachar, The Mann-Whitney U: a test for assessing whether two independent samples come from the same distribution, *Tutor Quant Methods Psychol* 4 (1) (2008) 13–20.
- [47] A.A. Moustafa, et al., Motor symptoms in Parkinson's disease: a unified framework, *Neurosci. Biobehav. Rev.* 68 (2016) 727–740.